636 *Inorg. Chem.* **2011**, *50*, 636–646
DOI: 10.1021/ic101847b

Inorganic Chemistry
Article

Comparison of the Redox Chemistry of Primary and Secondary Amides of U(IV): Isolation of a U(VI) Bis(imido) Complex or a Homoleptic U(VI) Amido Complex

Lani A. Seaman, Skye Fortier, Guang Wu, and Trevor W. Hayton*

Department of Chemistry and Biochemistry, University of California Santa Barbara, Santa Barbara, California 93106, United States

Received September 8, 2010

Reaction of UCl_4 with 6 equiv of $LiNH^tBu$ generates the U(IV) homoleptic amide complex $[Li(THF)_2Cl]_2[Li]_2[U(NH^tBu)_6]$ (**1**·THF) in 57% yield. In the solid-state, **1**·THF exists as a one-dimensional coordination polymer consisting of alternating $[Li]_2[U(NH^tBu)_6]$ and $[Li(THF)_2Cl]_2$ building blocks. Recrystallization of **1**·THF from DME/hexanes affords the monomeric DME derivative, $[Li(DME)_2ClLi]_2[U(NH^tBu)_6]$ (**1**·DME), which was also characterized by X-ray crystallography. The oxidation of **1**·THF with 1 equiv of AgOTF generates the U(VI) bis(imido) complex $[Li(THF)]_2[U(N^tBu)_2(NH^tBu)_4]$ (**2**) in low yield. In contrast, oxidation of **1**·THF with 1 equiv of I_2, in the presence of excess *tert*-butylamine, cleanly affords the U(VI) bis(imido) $U(N^tBu)_2(NH^tBu)_2(NH_2{}^tBu)_2$ (**3**) in 78% yield. We have also explored the reactivity of UCl_4 with the lithium salt of a secondary amide. Thus, reaction of 6 equiv of ($LiNC_5H_{10}$) (HNC_5H_{10} = piperidine) with UCl_4 in DME produces the U(IV) amide, $[Li(DME)][U(NC_5H_{10})_5]$ (**4**). Oxidation of this material with 0.5 equiv of I_2, followed by addition of $Li(NC_5H_{10})$, produces $[Li(DME)_3][U(NC_5H_{10})_6]$ (**5**) in moderate yield. Oxidation of **5** with 0.5 equiv of I_2 generates $U(NC_5H_{10})_6$ (**6**) in good yield. The structures of **4**−**6** were elucidated by X-ray crystallographic analysis, while the magnetic properties of **4** and **5** were investigated by SQUID magnetometry. Additionally, the solution phase redox properties of **5** were examined by cyclic voltammetry.

Introduction

The extent to which the actinides participate in covalent-bonding remains an open question and an active area of research.[1−15] At the heart of this issue is the ability of the 5f and 6d valence orbitals to engage in bonding. Computational modeling alone is not sufficient to explore this question, as DFT calculations are known to overestimate covalency in metal−ligand interactions,[5,16] even in less-challenging transition metal systems.[17] Consequently, a comprehensive understanding of actinide-ligand bonding requires a broad-ranging investigation into the synthesis and spectroscopic properties of molecular 5f-systems. A variety of experimental techniques have already been brought to bear on this problem,[1,18−20] including recently the use of ligand K-edge absorption spectroscopy,[5] and these studies are beginning to reveal a more definitive picture of actinide-ligand interactions. However, there are many areas where our understanding of uranium-ligand bonding could be improved, and this is especially true

*To whom correspondence should be addressed. E-mail: hayton@chem.ucsb.edu.

(1) Denning, R. G.; Green, J. C.; Hutchings, T. E.; Dallera, C.; Tagliaferri, A.; Giarda, K.; Brookes, N. B.; Braicovich, L. *J. Chem. Phys.* **2002**, *117*, 8008–8021.
(2) Denning, R. G. *J. Phys. Chem. A* **2007**, *111*, 4125–4143.
(3) Prodan, I. D.; Scuseria, G. E.; Martin, R. L. *Phys. Rev. B* **2007**, *76*, 033101.
(4) Arnold, P.; Turner, Z.; Kaltsoyannis, N.; Pelekanaki, P.; Bellabarba, R.; Tooze, R. *Chem.—Eur. J.* **2010**, *16*, 9623–9629.
(5) Kozimor, S. A.; Yang, P.; Batista, E. R.; Boland, K. S.; Burns, C. J.; Clark, D. L.; Conradson, S. D.; Martin, R. L.; Wilkerson, M. P.; Wolfsberg, L. E. *J. Am. Chem. Soc.* **2009**, *131*, 12125–12136.
(6) Cantat, T.; Graves, C. R.; Jantunen, K. C.; Burns, C. J.; Scott, B. L.; Schelter, E. J.; Morris, D. E.; Hay, P. J.; Kiplinger, J. L. *J. Am. Chem. Soc.* **2008**, *130*, 17537–17551.
(7) Li, J.; Bursten, B. E. *J. Am. Chem. Soc.* **1997**, *119*, 9021–9032.
(8) Tassell, M. J.; Kaltsoyannis, N. *Dalton Trans.* **2010**, *39*, 6719–6725.
(9) Ingram, K. I. M.; Kaltsoyannis, N.; Gaunt, A. J.; Neu, M. P. *J. Alloys Compd.* **2007**, *444*−*445*, 369–375.
(10) Ingram, K. I. M.; Tassell, M. J.; Gaunt, A. J.; Kaltsoyannis, N. *Inorg. Chem.* **2008**, *47*, 7824–7833.
(11) Gaunt, A. J.; Reilly, S. D.; Enriquez, A. E.; Scott, B. L.; Ibers, J. A.; Sekar, P.; Ingram, K. I. M.; Kaltsoyannis, N.; Neu, M. P. *Inorg. Chem.* **2007**, *46*, 29–41.
(12) Jensen, M. P.; Bond, A. H. *J. Am. Chem. Soc.* **2002**, *124*, 9870–9877.
(13) Mazzanti, M.; Wietzke, R. l.; Pecaut, J.; Latour, J.-M.; Maldivi, P.; Remy, M. *Inorg. Chem.* **2002**, *41*, 2389–2399.
(14) Arliguie, T.; Belkhiri, L.; Bouaoud, S.-E.; Thuery, P.; Villiers, C.; Boucekkine, A.; Ephritikhine, M. *Inorg. Chem.* **2008**, *47*, 221–230.
(15) Roger, M.; Belkhiri, L.; Arliguie, T.; Thuery, P.; Boucekkine, A.; Ephritikhine, M. *Organometallics* **2007**, *26*, 33–42.
(16) Atanasov, M.; Daul, C.; Gudel, H. U.; Wesolowski, T. A.; Zbiri, M. *Inorg. Chem.* **2005**, *44*, 2954–2963.
(17) Szilagyi, R. K.; Metz, M.; Solomon, E. I. *J. Phys. Chem. A* **2002**, *106*, 2994–3007.
(18) Bradley, J. A.; Sen Gupta, S.; Seidler, G. T.; Moore, K. T.; Haverkort, M. W.; Sawatzky, G. A.; Conradson, S. D.; Clark, D. L.; Kozimor, S. A.; Boland, K. S. *Phys. Rev. B* **2010**, *81*, 4.
(19) Iversen, B. B.; Larsen, F. K.; Pinkerton, A. A.; Martin, A.; Darovsky, A.; Reynolds, P. A. *Inorg. Chem.* **1998**, *37*, 4559–4566.
(20) Beach, D. B.; Bomben, K. D.; Edelstein, N. M.; Eisenberg, D. C.; Jolly, W. L.; Shinomoto, R.; Streitwieser, A. *Inorg. Chem.* **1986**, *25*, 1735–1737.

 Published on Web 12/13/2010 © 2010 American Chemical Society

for the bonding in high-valent uranium. Uranium possesses a range of chemically accessible oxidation states, from 3+ to 6+, but the observation of the 5+ and 6+ states is generally limited to complexes containing the uranyl fragment, UO_2^{n+} (n = 1, 2).[21−23] Indeed, U(VI) complexes that do not possess the uranyl moiety are relatively rare, and largely restricted to a small number of U(VI) halides, alkoxides, and imido complexes.[24,25]

Our laboratory has recently employed the strategy of "-ate" complex formation to access stable uranium(IV) precursors which are readily amenable to oxidation.[26−28] For example, addition of 6 equiv of lithium *tert*-butoxide to UCl_4 provides the sterically saturated U(IV) uranate $[Li(THF)]_2[U(O^tBu)_6]$.[27] The coordination of the six *tert*-butoxide groups to U^{4+} allows for facile oxidation to both U(V) and U(VI). This strategy was also successful in generating several thermally stable homoleptic U(IV) alkyl complexes.[28,29] We have now applied this methodology to the synthesis of homoleptic uranium amide complexes, with the goal of isolating new examples of high-valent uranium. Although low valent uranium amides have been known since the Manhattan project,[30] very few examples of amides in higher oxidation states have been reported.[31,32] This may be due to the belief that lithium and sodium amide reagents would readily reduce a high-valent uranium ion.[33] Nonetheless, a few high-valent uranium amides are known. For example, reaction of $UI_3(THF)_4$ with Li(dbabh) produces the U(V) amide complex $[Li(THF)_x][U(dbabh)_6]$ (Hdbabh = 2,3:5,6-dibenzo-7-azabicyclo[2.2.1]hepta-2,5-diene), which can be further oxidized to $U(dbabh)_6$.[34] Both of these complexes have been structurally characterized. Additionally, the U(V) amides $[Li(THF)][U(NMe_2)_6]$ and $U(NEt_2)_5$, and a U(VI) derivative, $U(NMe_2)_6$, have also been reported.[31] However, these materials have only received brief mention in the literature and have not been fully characterized. Herein, we describe our efforts to synthesize a series of homoleptic uranium(V) and uranium(VI) amides, by employing either primary and secondary amides as co-ligands.

Results and Discussion

Addition of 6 equiv of $LiNH^tBu$ to UCl_4 in tetrahydrofuran (THF) results in formation of an orange-brown solution. Filtration of the reaction mixture and crystallization from THF/DME/hexane, in a 3:1:3 ratio, affords the U(IV) amide complex $[Li(THF)_2Cl]_2[Li]_2[U(NH^tBu)_6]$ (**1**·THF) as orange crystals in 57% yield (eq 1). We have found the addition of DME for crystallization is essential, as isolation from only THF/hexanes results in significantly lower yields. Additionally, reaction of UCl_4 with only 4 equiv of $LiNH^tBu$ produces an intractable mixture.

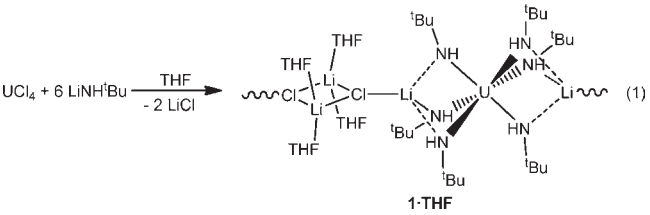

(1)

In the solid-state, **1**·THF crystallizes in the monoclinic space group $P2_1/n$ as a one-dimensional (1D) coordination polymer with one uranium atom in the asymmetric unit (Figure 1). Each uranium center in **1**·THF is ligated by six *tert*-butyl amide groups in a distorted octahedral geometry (e.g., N1−U1−N2 = 81.0(2)°, N1−U1−N3 = 99.0(2)°). Additionally, two lithium cations are contained within its secondary coordination sphere, each ligated by three nitrogen atoms of the *tert*-butyl amide groups, resulting in the formation of the $[Li]_2[U(NH^tBu)_6]$ moiety. Complex **1**·THF also incorporates two molecules of LiCl into its structure, which are arranged as a THF-stabilized dimer, namely, $[Li(THF)_2Cl]_2$. The 1D polymer chain is built from alternating $[Li(THF)_2Cl]_2$ and $[Li]_2[U(NH^tBu)_6]$ units, and the two subunits are connected via a Li−Cl dative interaction. The U−N bond lengths in **1**·THF range from U1−N3 = 2.352(6) Å to U1−N1 = 2.368(6) Å, while the U−N−C bond angles range from U1−N1−C1 = 145.0(5)° to U1−N3−C3 = 146.0(5)°. Notably, the U−N distances in **1**·THF (av. 2.36(1) Å) are significantly longer than the $U-N_{amide}$ distances (av. 2.20(2) Å) found for the related U(IV) amide $[(^tBuNH_2)_3(^tBuNH)_3U][BPh_4]$.[35] The longer U−N distances in **1**·THF are likely due to the bridging interaction of the *tert*-butyl amide ligands with the lithium cations. Finally, the Li−N bond distances (Li1−N1 = 2.19 (1) Å, Li1−N2 = 2.19(1) Å, Li1−N3 = 2.18(1) Å) are typical of Li−N bond lengths in metal amide complexes.[36]

Complex **1**·THF is insoluble in hexanes, sparingly soluble in Et_2O and aromatic solvents, but completely soluble in THF. The ^1H NMR spectrum of **1**·THF in C_6D_6 exhibits two singlets at −20.42 ppm and 2.10 ppm, in a 1:9 ratio, assignable to the N−H and methyl protons of the *tert*-butyl amide ligand, respectively. The $^7Li\{^1H\}$ NMR spectrum displays one resonance at 0.93 ppm, suggesting rapid exchange between the two inequivalent Li environments. It should be noted that upon dissolution in C_6D_6, samples of **1**·THF show immediate signs of decomposition, as evidenced by the appearance of several new resonances in the ^1H NMR spectrum, and the appearance of a new resonance at 48.9 ppm in the $^7Li\{^1H\}$ NMR spectrum. These peaks

(21) Morss, L. R., Edelstein, N. M., Fuger, J., Katz, J. J., Eds.; *The Chemistry of the Actinide and Transactinide Elements*; Springer: New York, 2006.
(22) Graves, C. R.; Kiplinger, J. L. *Chem. Commun.* **2009**, 3831–3853.
(23) Arnold, P. L.; Love, J. B.; Patel, D. *Coord. Chem. Rev.* **2009**, *253*, 1973–1978.
(24) Cotton, S. *Lanthanide and Actinide Chemistry*; John Wiley & Sons, Ltd.: West Sussex, England, 2006.
(25) Hayton, T. W. *Dalton Trans.* **2010**, 1145–1158.
(26) Seaman, L. A.; Schnaars, D. D.; Wu, G.; Hayton, T. W. *Dalton Trans.* **2010**, *39*, 6635–6637.
(27) Fortier, S.; Wu, G.; Hayton, T. W. *Inorg. Chem.* **2008**, *47*, 4752–4761.
(28) Fortier, S.; Melot, B. C.; Wu, G.; Hayton, T. W. *J. Am. Chem. Soc.* **2009**, *131*, 15512–15521.
(29) Sigurdson, E. R.; Wilkinson, G. *J. Chem. Soc., Dalton Trans.* **1977**, 812–818.
(30) Jones, R. G.; Karmas, G.; Martin, G. A.; Gilman, H. *J. Am. Chem. Soc.* **1956**, *78*, 4285–4286.
(31) Berthet, J. C.; Ephritikhine, M. *Coord. Chem. Rev.* **1998**, *178−180*, 83–116.
(32) Ephritikhine, M.; Berthet, J. C.; Boisson, C.; Lance, M.; Nierlich, M. *J. Alloys Compd.* **1998**, *271−273*, 144–149.
(33) Burns, C. J.; Clark, D. L.; Donohoe, R. J.; Duval, P. B.; Scott, B. L.; Tait, C. D. *Inorg. Chem.* **2000**, *39*, 5464–5468.
(34) Meyer, K.; Mindiola, D. J.; Baker, T. A.; Davis, W. M.; Cummins, C. C. *Angew. Chem., Int. Ed.* **2000**, *39*, 3063–3066.
(35) Wang, J.; Dash, A. K.; Kapon, M.; Berthet, J.-C.; Ephritikhine, M.; Eisen, M. S. *Chem.—Eur. J.* **2002**, *8*, 5384–5396.
(36) Pauer, F.; Power, P. P. Structures of Lithium Salts and Heteroatom Compounds. In *Lithium Chemistry: A Theoretical and Experimental Overview*; Sapse, A. M., von Ragué Schleyer, P., Eds.; John Wiley & Sons, Inc: New York, 1995; pp 295−392.

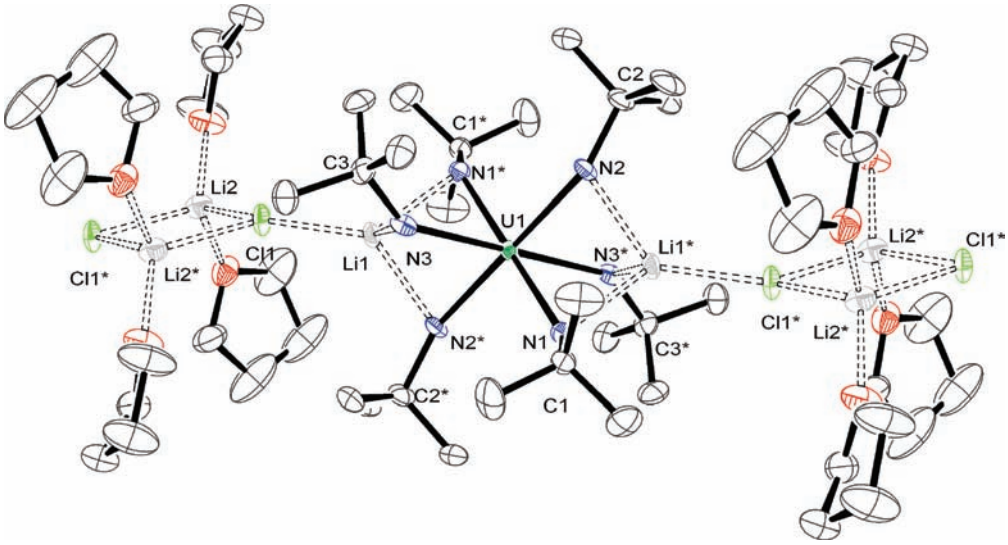

Figure 1. ORTEP diagram of a portion of the 1D chain observed for $[Li(THF)_2Cl]_2[Li]_2[U(NH^tBu)_6]$ (**1**·THF) with 50% probability ellipsoids. Asterisks indicate symmetry related atoms. Selected bond lengths (Å) and bond angles (deg): U1−N1 = 2.368(6), U1−N2 = 2.362(6), U1−N3 = 2.352(6), Li1−N1 = 2.19 (1), Li1−N2 = 2.19(1), Li1−N3 = 2.18(1), Li1−Cl1 = 2.34(1), Li2−Cl1 = 2.37(1), U1−N1−C1 = 145.0(5), U1−N2−C2 = 145.1(5), U1−N3−C3 = 146.0(5), N1−U1−N2 = 81.0(2), N1−U1−N3 = 99.0(2), N1−U1−N1* = 180, N1−U1−N2* = 99.0(2), N1−U1−N3* = 81.0(2).

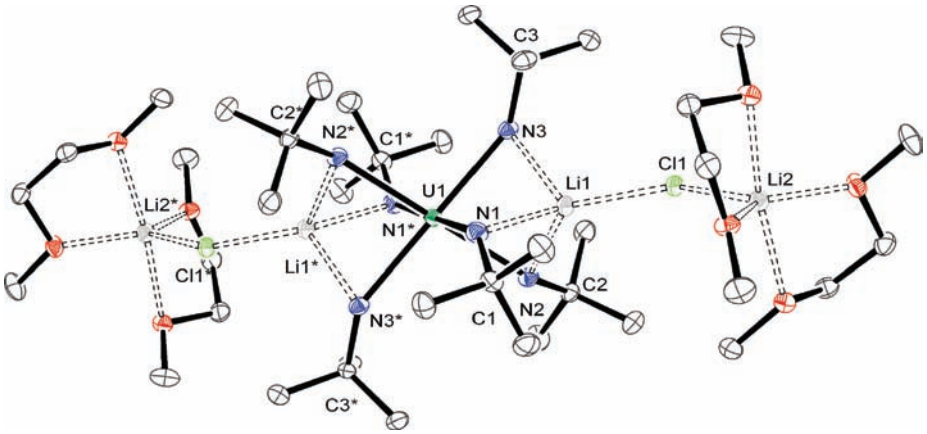

Figure 2. ORTEP diagram of $[Li(DME)_2ClLi]_2[U(NH^tBu)_6]$ (**1**·DME·C_6H_{14}) with 50% probability ellipsoids. Asterisks indicate symmetry related atoms. Selected bond lengths (Å) and bond angles (deg): U1−N1 = 2.364(4), U1−N2 = 2.384(4), U1−N3 = 2.371(4), Li1−N1 = 2.258(9), Li1−N2 = 2.210(9), Li1−N3 = 2.173(9), Li1−Cl1 = 2.327(8), Li2−Cl1 = 2.349(8), U1−N1−C1 = 147.2(3), U1−N2−C2 = 144.1(3), U1−N3−C3 = 144.7(3), N1−U1−N2 = 81.4(1), N1−U1−N3 = 82.8(1), N1−U1−N1* = 180, N1−U1−N2* = 98.6(1), N1−U1−N3* = 97.2(1).

grow over time and after two days no resonances attributable to **1**·THF are observable. Likewise, THF-d_8 solutions of **1**·THF decompose over the course of a day. Addition of 12-crown-4 to solutions of **1**·THF only results in the formation of an intractable mixture.

Incorporation of the $[Li(THF)_2Cl]_2$ moiety into an "ate" complex has been previously reported.[37−41] From a synthetic standpoint, this is non-ideal, and we have made several attempts to remove the co-crystallized LiCl, including recrystallization from other solvents. For instance, recrystallization from DME/hexanes affords crystals of a new material, $[Li(DME)_2ClLi]_2[U(NH^tBu)_6]$ (**1**·DME), but fails to remove any of the co-crystallized LiCl. Complex **1**·DME crystallizes in the triclinic space group $P\bar{1}$ as the hexanes solvate **1**·DME·C_6H_{14}, and its solid-state molecular structure is shown in Figure 2. Complex **1**·DME·C_6H_{14} exists as a monomer and exhibits a distorted octahedral geometry around the uranium center (e.g., N1−U1−N2 = 81.4(1)°, N1−U1−N2* = 98.6(1)°). As with **1**·THF, 2 equiv of LiCl are incorporated into the complex; however, the two LiCl molecules have been rearranged to produce two $[ClLiCl]^+$ cations. One end of the $[LiClLi]^+$ cation is coordinated by three amide nitrogen atoms, while two molecules of DME cap the other end of the $[LiClLi]^+$ unit. The amide bond lengths range from U1−N1 = 2.364(4) Å to U1−N2 = 2.384(4) Å, which are similar to the amide bond lengths seen in **1**·THF. Its other metrical parameters are also comparable.

While we were unable to remove the 2 equiv of LiCl from **1**·THF, we still endeavored to investigate its oxidation

(37) Schmuck, A.; Leopold, D.; Wallenhauer, S.; Seppelt, K. *Chem. Ber.* **1990**, *123*, 761–766.
(38) Solari, E.; De Angelis, S.; Floriani, C.; Chiesi-Villa, A.; Rizzoli, C. *Inorg. Chem.* **1992**, *31*, 96–101.
(39) Ho, J.; Hou, Z.; Drake, R. J.; Stephan, D. W. *Organometallics* **1993**, *12*, 3145–3157.
(40) Tayebani, M.; Gambarotta, S.; Yap, G. *Organometallics* **1998**, *17*, 3639–3641.
(41) Bickley, J. F.; Copsey, M. C.; Jeffery, J. C.; Leedham, A. P.; Russell, C. A.; Stalke, D.; Steiner, A.; Stey, T.; Zacchini, S. *Dalton Trans.* **2004**, 989–995.

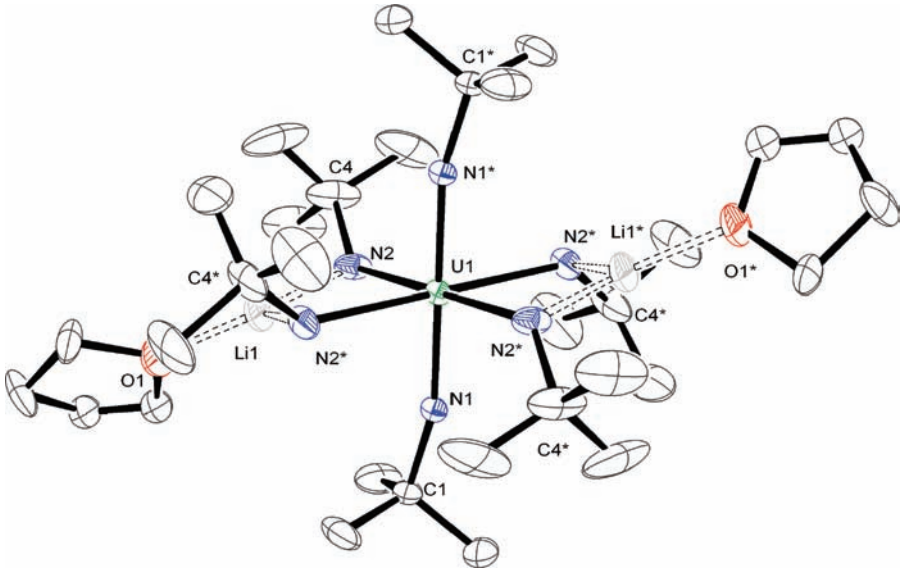

Figure 3. ORTEP diagram of $[Li(THF)]_2[U(N^tBu)_2(NH^tBu)_4]$ (**2**) with 50% probability ellipsoids. Asterisks indicate symmetry related atoms. Selected bond lengths (Å) and angles (deg): U1−N1 = 1.915(5), U1−N2 = 2.401(4), Li1−N2 = 2.008(9), U1−N1−C1 = 164.8(4), U1−N2−C4 = 135.7(3), N1−U1−N2 = 85.3(1), N1−U1−N1* = 180, N1−U1−N2* = 94.7(1).

Scheme 1

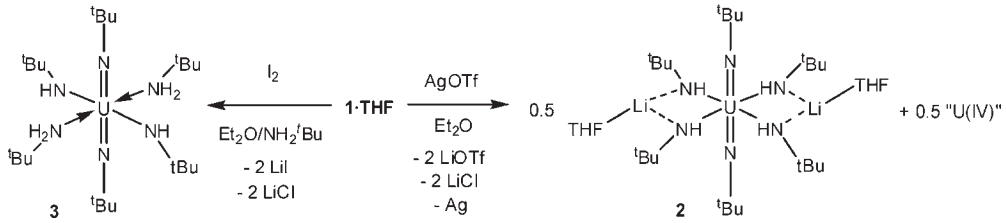

chemistry. Thus, addition of 1 equiv of AgOTf to an Et_2O suspension of **1**·THF results in precipitation of silver metal and formation of a dark brown solution. From the reaction mixture, the U(VI) bis(imido) complex $[Li(THF)]_2[U(N^tBu)_2(NH^tBu)_4]$ (**2**) can be isolated in 33% yield (Scheme 1). The ^1H NMR spectrum of **2** in C_6D_6 exhibits resonances at 2.06 ppm and 1.08 ppm, in a 2:1 ratio. These can be assigned to the *tert*-butyl groups of the equatorial amido ligands and the axial imido ligands, respectively. The $^7Li\{^1H\}$ NMR spectrum of **2** exhibits a singlet at 1.52 ppm. Complex **2** is insoluble in non-polar solvents but very soluble in Et_2O and THF. Unfortunately, the LiOTf byproduct generated in the reaction possesses similar solubility properties, and the inclusion of residual LiOTf in samples of **2** has precluded a satisfactory elemental analysis.

Crystals of **2** suitable for X-ray crystallographic analysis were grown from an Et_2O/hexane solution. Complex **2** crystallizes in the monoclinic space group *C*2/*m*, and its solid-state molecular structure is shown in Figure 3. In the solid-state, **2** exhibits a distorted octahedral geometry about the uranium center (e.g., N1−U1−N2 = 85.3(1)°, N1−U1−N2* = 94.7(1)°). The two imido ligands in **2** exhibit a *trans* configuration, while the equatorial plane consists of four *tert*-butyl amide groups. Additionally, its two lithium cations are ligated by two *tert*-butyl amide ligands and one THF molecule, affording each a trigonal planar geometry. Complex **2** possesses a $U-N_{imido}$ bond length of U1−N1 = 1.915(5) Å and a nearly linear $U-N_{imido}-C$ angle of U1−N1−C1 = 164.8(4)°. The $U-N_{amide}$ bond length (U1−N2 = 2.401(4) Å) is considerably longer and possesses a smaller $U-N_{amide}-C$ bond angle (U1−N2−C4 = 135.7(3)°). Finally, the Li−N bond length is Li1−N2 = 2.008(9) Å, which is slightly shorter than those observed for **1**·THF.

Uranium bis(imido) complexes, which can be found in both *cis*[42−47] and *trans*[48−52] configurations, have received increased attention in recent years. The *trans*-$[U(NR)_2]^{2+}$ complexes, which are analogues of the better known UO_2^{2+} cation, are characterized by short $U-N_{imido}$ bond lengths (ca. 1.84 Å). Interestingly, the $U-N_{imido}$ bond length in **2** is longer than the U−N bond lengths observed previously for

(42) Arney, D. S. J.; Burns, C. J.; Smith, D. C. *J. Am. Chem. Soc.* **1992**, *114*, 10068–10069.
(43) Arney, D. S. J.; Burns, C. J. *J. Am. Chem. Soc.* **1995**, *117*, 9448–9460.
(44) Warner, B. L.; Scott, B. L.; Burns, C. J. *Angew. Chem., Int. Ed.* **1998**, *37*, 959–960.
(45) Peters, R. G.; Warner, B. P.; Scott, B. L.; Burns, C. J. *Organometallics* **1999**, *18*, 2587–2589.
(46) Peters, R. G.; Warner, B. P.; Burns, C. J. *J. Am. Chem. Soc.* **1999**, *121*, 5585–5586.
(47) Evans, W. J.; Traina, C. A.; Ziller, J. W. *J. Am. Chem. Soc.* **2009**, *131*, 17473–17481.
(48) Hayton, T. W.; Boncella, J. M.; Scott, B. L.; Palmer, P. D.; Batista, E. R.; Hay, P. J. *Science* **2005**, *310*, 1941–1943.
(49) Hayton, T. W.; Boncella, J. M.; Scott, B. L.; Batista, E. R.; Hay, P. J. *J. Am. Chem. Soc.* **2006**, *128*, 10549–10559.
(50) Spencer, L. P.; Yang, P.; Scott, B. L.; Batista, E. R.; Boncella, J. M. *J. Am. Chem. Soc.* **2008**, *130*, 2930–2931.
(51) Spencer, L. P.; Schelter, E. J.; Yang, P.; Gdula, R. L.; Scott, B. L.; Thompson, J. D.; Kiplinger, J. L.; Batista, E. R.; Boncella, J. M. *Angew. Chem., Int. Ed.* **2009**, *48*, 3795–3798.
(52) Spencer, L. P.; Yang, P.; Scott, B. L.; Batista, E. R.; Boncella, J. M. *Inorg. Chem.* **2009**, *48*, 11615–11623.

Scheme 2

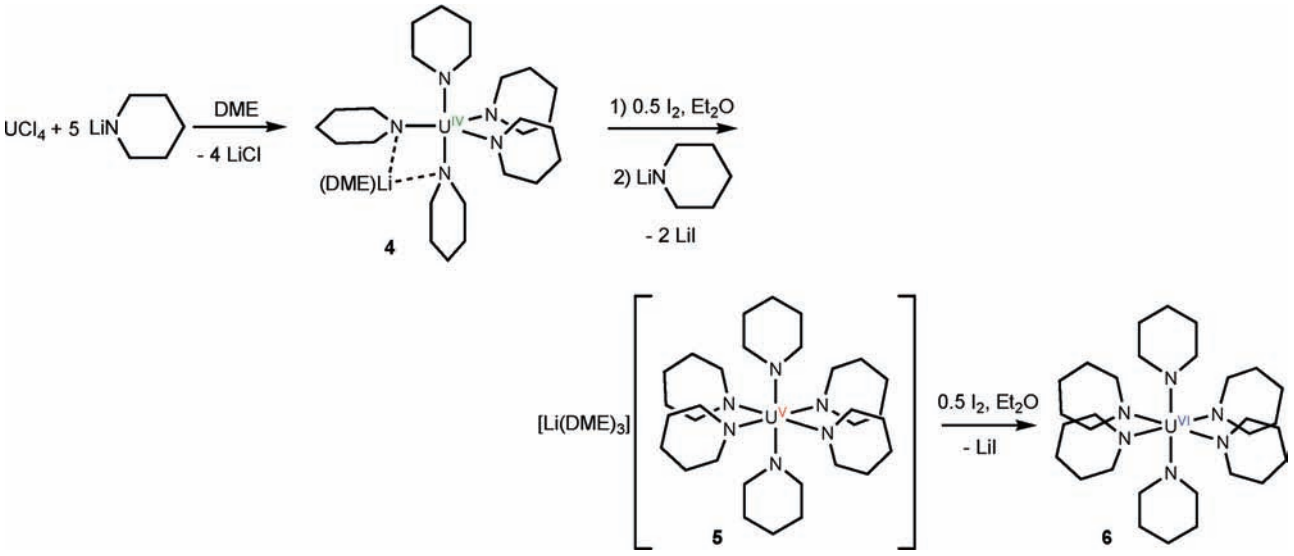

this class of materials.[48] This may be due to the coordination of four strongly electron-donating *tert*-butyl amide ligands to the uranium center. It has previously been shown that coordination of electron-donating ligands such as amides[53,54] and alkoxides[55] to the equatorial plane of the uranyl ion results in a lengthening of the U=O bond.[56]

No evidence for the formation of a U(V) complex is observed in the reaction mixture, despite the use of only 1 equiv of AgOTf, which further demonstrates the thermodynamic stability of the *trans*-bis(imido) geometry.[49] Additionally, the reaction of **1**·THF with 2 equiv of AgOTf does not result in a higher yield of **2**, but instead affords an intractable mixture. During the formation of **2**, the deprotonation of two amido groups is required to generate the *trans*-bis(imido) framework. This is probably accomplished by sacrificing an equiv of **1**·THF for use as an external base. Accordingly, the maximum yield of **2** can only be 50% (Scheme 1). Attempts to improve the yield of **2** by purposeful addition of NEt_3 have not proven fruitful. However, we have found that the oxidation of **1**·THF with 1 equiv of I_2, in the presence of excess *tert*-butyl amine, cleanly produces a new bis(imido) complex, namely, $U(N^tBu)_2(NH^tBu)_2(NH_2^tBu)_2$ (**3**) (Scheme 1). Interestingly, complex **3** is a structural isomer of the original target complex, the U(VI) hexa(amide) $U(NH^tBu)_6$.

Complex **3** can be isolated in 78% yield as an orange-red microcrystalline solid by crystallization from hexane. Consistent with its formulation, the ^{1}H NMR spectrum of **3** in C_6D_6 exhibits three *tert*-butyl resonances at 0.90 ppm, 1.50 ppm, and 1.97 ppm, in a 1:1:1 ratio. The resonance at 0.90 ppm is sharp and is assignable to methyl protons of the *tert*-butyl imido group, while the peaks at 1.50 ppm and 1.97 ppm are broad. We have assigned these latter resonances to the protons of the *tert*-butyl amine and *tert*-butyl amide ligands, respectively. In support of this assignment, addition of excess *tert*-butyl amine to a C_6D_6 solution of **3** results in the disappearance of the resonance at 1.50 ppm and the appearance of a new resonance at 1.04 ppm, while leaving the peaks at 1.97 ppm and 0.90 ppm unchanged.

The proton transfer required to generate the imido ligands in **3** may occur via an internal proton transfer between two amide ligands, resulting in concomitant formation of a *tert*-butyl amine ligand and a *tert*-butyl imido group. It is also possible that the excess *tert*-butyl amine in the reaction mixture is involved in an intermolecular proton transfer. While its exact role is not known, the excess *tert*-butyl amine is necessary for successful isolation of **3**. With no *tert*-butyl amine in the reaction mixture, the only identifiable material formed between **1**·THF and I_2 is complex **2**, which is generated in low yields.

The formation of the imido-containing complexes **2** and **3**, upon oxidation of **1**·THF with either AgOTf or I_2, suggests that the isolation of a stable U(VI) hexakis(amide) requires the use of a secondary amide. As a result, we have explored the reactivity of lithium piperidide ($LiNC_5H_{10}$) with UCl_4. Thus, reaction of UCl_4 with 6 equiv of $LiNC_5H_{10}$ in Et_2O/DME generates a deep blue-green solution, from which the pentacoordinate U(IV) complex $[Li(DME)][U(NC_5H_{10})_5]$ (**4**) can be isolated as blue-green crystals in 62% yield (Scheme 2). Addition of 5 equiv of $LiNC_5H_{10}$ to UCl_4 also provides **4** in comparable yields, while addition of only 4 equiv of $LiNC_5H_{10}$ to UCl_4 generates an intractable mixture. Complex **4** is insoluble in non-polar solvents such as hexane but is very soluble in aromatic and ethereal solvents. The ^{1}H NMR spectrum of **4** in C_6D_6 exhibits an extremely broad resonance at 6.24 ppm, which we have assigned to the protons of the piperidide ring. Its ^{7}Li{^{1}H} NMR spectrum displays a single resonance at 81.2 ppm.

Storage of a concentrated DME/hexane solution of **4** at −25 °C for several hours affords material suitable for X-ray crystallographic analysis. Complex **4** crystallizes in the noncentrosymmetric hexagonal space group $P3_2$, and its solid-state molecular structure is shown in Figure 4. In the solid-state, **4** adopts a trigonal bipyramidal geometry about uranium. The single lithium cation is ligated by two piperidide nitrogen atoms and one DME molecule, affording it a tetrahedral

(53) Sarsfield, M. J.; Helliwell, M.; Raftery, J. *Inorg. Chem.* **2004**, *43*, 3170–3179.
(54) Burns, C. J.; Clark, D. L.; Donohoe, R. J.; Duval, P. B.; Scott, B. L.; Tait, C. D. *Inorg. Chem.* **2000**, *39*, 5464–5468.
(55) Wilkerson, M. P.; Burns, C. J.; Dewey, H. J.; Martin, J. M.; Morris, D. E.; Paine, R. T.; Scott, B. L. *Inorg. Chem.* **2000**, *39*, 5277–5285.
(56) Fortier, S.; Hayton, T. W. *Coord. Chem. Rev.* **2010**, *254*, 197–214.

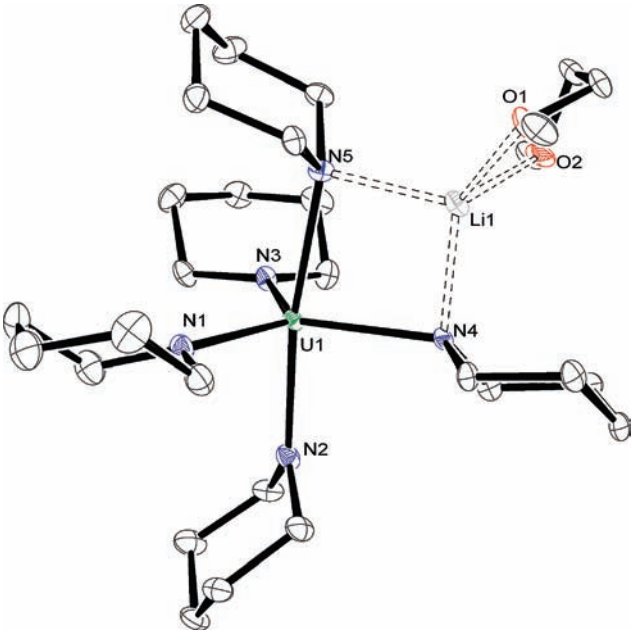

Figure 4. ORTEP diagram of $[Li(DME)][U(NC_5H_{10})_5]$ (**4**) with 50% probability ellipsoids. Selected bond lengths (Å) and angles (deg): U1−N1 = 2.262(9), U1−N2 = 2.274(9), U1−N3 = 2.238(9), U1−N4 = 2.370(8), U1−N5 = 2.388(9), Li1−N4 = 2.04(2), Li1−N5 = 2.09(2), Li1−O1 = 1.98(2), Li1−O2 = 2.04(2), N1−U1−N2 = 91.7(3), N1−U1−N3 = 122.8(3), N1−U1−N4 = 118.1(3), N1−U1−N5 = 96.2(3). Sum of angles around nitrogen atoms: N1 = 357(2)°, N2 = 360(1)°, N3 = 358(1)°.

geometry. The U−N bond lengths of the terminal piperidide groups are U1−N1 = 2.262(9) Å, U1−N2 = 2.274(9) Å, and U1−N3 = 2.238(9) Å, whereas the U−N bonds of the bridging piperidide ligands are longer at U1−N4 = 2.370(8) Å and U1−N5 = 2.388(9) Å. The terminal U−N bond lengths of **4** are comparable to those normally observed for U(IV) amide complexes,[31] while the bridging U−N distances are similar to those observed for **1**·THF. The sum of angles about the nitrogen atoms of the terminal amide ligands range from 357(2)° to 360(1)°, consistent with sp^2 hybridization at nitrogen. Terminal dialkylamide ligands possessing planar nitrogen atoms have also been observed in other U(IV) systems, including $[U(NEt_2)_4]_2$.[57−59]

The inability of complex **4** to coordinate a sixth piperidide ligand is likely not due to sterics, as evidenced by the isolation of the octahedral U^{5+} piperidide complex, $[Li(DME)_3][U(NC_5H_{10})_6]$ (vide infra). Therefore, we believe that the strongly electron donating piperidide ligands impart a significant negative charge on the U^{4+} ion in **4**, disfavoring the coordination of a sixth piperidide ligand, simply via electrostatic repulsion. This rationale also explains the pentacoordinate structures of $[Li][UR_5]$ (R = $CH_2{}^tBu$, CH_2SiMe_3), in which the U^{4+} ion is also ligated by five potent electron-donating ligands.[28]

To better assess the electronic structure of **4**, its magnetic susceptibility was measured using SQUID magnetometry. A plot of its effective magnetic moment (μ_{eff}) versus temperature is shown in Figure 5. At 295 K, **4** exhibits a μ_{eff} of 3.18 μ_B, which is smaller than the 3.58 μ_B expected for a free $5f^2$ ion possessing a $^3H_4$ ground state.[60−62] The related U(IV) amide complex $[U(NEt_2)_4]_2$ possesses a similar μ_{eff} (2.81 μ_B).[57] Lower effective magnetic moments for U^{4+} are usually attributed to covalent metal−ligand interactions, which quench angular orbital momentum,[62−67] or the presence of a strong ligand field.[61,64,68−73] Interestingly, the effective magnetic moment in **4** is relatively independent of temperature. Upon cooling to 20 K, the effective magnetic moment of **4** drops only slightly to 3.06 μ_B, before quickly decreasing to 1.81 μ_B at 2 K. This temperature response differs markedly from the strong temperature dependence of μ_{eff} normally observed for U^{4+}.[28,61,62,64,66,71,74−77] However, the magnetic behavior of **4** is comparable to that observed for the isostructural pentacoordinate U(IV) alkyls $[Li][UR_5]$ (R = $CH_2{}^tBu$, CH_2SiMe_3).[28]

Attempts to oxidize **4** with I_2 or AgOTf only produce complex reaction mixtures. However, clean transformation of **4** into a U(V) amide can be achieved by oxidation with 0.5 equiv of I_2, followed by addition of 1 equiv of $LiNC_5H_{10}$ (Scheme 2). This generates a deep red solution from which the six-coordinate homoleptic U(V) amide $[Li(DME)_3][U(NC_5H_{10})_6]$ (**5**) can be isolated in 53% yield. The ^1H NMR spectrum of **5** in C_6D_6 exhibits two overlapping resonances at 2.48 ppm and 2.56 ppm assignable to the β- and γ-protons of the piperidide ligand, respectively. A third broad resonance, corresponding to the α-protons, appears at 11.59 ppm. Consistent with its formulation, the $^7Li\{^1H\}$ NMR spectrum of **5** contains a single resonance at 13.5 ppm.

Complex **5** crystallizes in the monoclinic space group $P2_1/n$ as a discrete cation/anion pair. The anionic U(V) center is coordinated by six piperidide ligands, affording it an octahedral geometry (Figure 6). The U−N bond lengths in **5** (U1−N1 = 2.292(6) Å, U1−N2 = 2.266(6) Å, U1−N3 = 2.250(6) Å, U1−N4 = 2.280(6) Å, U1−N5 = 2.283(6) Å,

(57) Reynolds, J. G.; Zalkin, A.; Templeton, D. H.; Edelstein, N. M.; Templeton, L. K. *Inorg. Chem.* **1976**, *15*, 2498–2502.
(58) Hitchcock, P. B.; Lappert, M. F.; Singh, A.; Taylor, R. G.; Brown, D. *J. Chem. Soc., Chem. Commun.* **1983**, 561–563.
(59) Berthet, J.-C.; Boisson, C.; Lance, M.; Vigner, J.; Nierlich, M.; Ephritikhine, M. *J. Chem. Soc., Dalton Trans.* **1995**, 3019–3025.
(60) Hutchison, C. A.; Elliot, N. *J. Chem. Phys.* **1948**, *16*, 920–927.
(61) Schelter, E. J.; Yang, P.; Scott, B. L.; Thompson, J. D.; Martin, R. L.; Hay, P. J.; Morris, D. E.; Kiplinger, J. L. *Inorg. Chem.* **2007**, *46*, 7477–7488.
(62) Castro-Rodriguez, I.; Olsen, K.; Gantzel, P.; Meyer, K. *J. Am. Chem. Soc.* **2003**, *125*, 4565–4571.
(63) Boudreaux, E. A.; Mulay, L. N. *Theory and Applications of Molecular Paramagnetism*; John Wiley & Sons: New York, 1976.
(64) Castro-Rodriguez, I.; Meyer, K. *Chem. Commun.* **2006**, 1353–1368.
(65) Bart, S. C.; Anthon, C.; Heinemann, F. W.; Bill, E.; Edelstein, N. M.; Meyer, K. *J. Am. Chem. Soc.* **2008**, *130*, 12536–12546.
(66) Bart, S. C.; Heinemann, F. W.; Anthon, C.; Hauser, C.; Meyer, K. *Inorg. Chem.* **2009**, *48*, 9419–9426.
(67) Monreal, M. J.; Carver, C. T.; Diaconescu, P. L. *Inorg. Chem.* **2007**, *46*, 7226–7228.
(68) Reynolds, J. G.; Zalkin, A.; Templeton, D. H.; Edelstein, N. M. *Inorg. Chem.* **1977**, *16*, 1090–1096.
(69) Stewart, J. L.; Andersen, R. A. *New J. Chem.* **1995**, *19*, 587–595.
(70) Graves, C. R.; Yang, P.; Kozimor, S. A.; Vaughn, A. E.; Clark, D. L.; Conradson, S. D.; Schelter, E. J.; Scott, B. L.; Thompson, J. D.; Hay, P. J.; Morris, D. E.; Kiplinger, J. L. *J. Am. Chem. Soc.* **2008**, *130*, 5272–5285.
(71) Schelter, E. J.; Veauthier, J. M.; Graves, C. R.; John, K. D.; Scott, B. L.; Thompson, J. D.; Pool-Davis-Tournear, J. A.; Morris, D. E.; Kiplinger, J. L. *Chem.—Eur. J.* **2008**, *14*, 7782–7790.
(72) Schelter, E. J.; Morris, D. E.; Scott, B. L.; Thompson, J. D.; Kiplinger, J. L. *Inorg. Chem.* **2007**, *46*, 5528–5536.
(73) Rinehart, J. D.; Harris, T. D.; Kozimor, S. A.; Bartlett, B. M.; Long, J. R. *Inorg. Chem.* **2009**, *48*, 3382–3395.
(74) Lam, O. P.; Bart, S. C.; Kameo, H.; Heinemann, F. W.; Meyer, K. *Chem. Commun.* **2010**, *46*, 3137–3139.
(75) Lam, O. P.; Anthon, C.; Heinemann, F. W.; Connor, J. M.; Meyer, K. *J. Am. Chem. Soc.* **2008**, *130*, 6567–6576.
(76) Lam, O. P.; Feng, P. L.; Heinemann, F. W.; O'Connor, J. M.; Meyer, K. *J. Am. Chem. Soc.* **2008**, *130*, 2806–2816.
(77) Kozimor, S. A.; Bartlett, B. M.; Rinehart, J. D.; Long, J. R. *J. Am. Chem. Soc.* **2007**, *129*, 10672–10674.

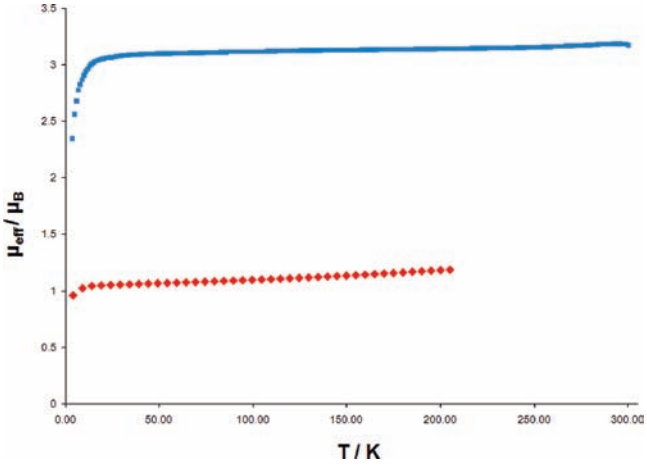

Figure 5. Temperature-dependent SQUID magnetization data for complexes **4** (blue line) and **5** (red line).

U1−N6 = 2.270(5) Å) are comparable to the terminal U−N bond lengths in **4** (U1−N1 = 2.262(9) Å), despite the presence of the smaller U^{5+} ion. They are also similar to those found in $[PPh_4][U(dbabh)_6]$ (Hdbabh = 2,3:5,6-dibenzo-7-azabicyclo-[2.2.1]hepta-2,5-diene), which range from 2.23(1) Å to 2.27(1) Å.[34] Additionally, the nitrogen atoms of the piperidide ligands in **5** display nearly planar geometries, similar to that observed for **4**. The other known homoleptic U(V) amides, $U(NEt_2)_5$ and $[Li][U(NMe_2)_6]$, have not been structurally characterized.[31,78]

Complex **5** is slightly soluble in hexanes but fully soluble in aromatic and ethereal solvents. Additionally, we have observed that the LiI byproduct, generated during the oxidation of **4**, is extremely persistent in samples of **5**. This may be due to the ability of the uranium-coordinated piperidide ligands to also ligate the Li^+ ion of lithium iodide. Nonetheless, we have found the removal of LiI can be achieved by adding a few drops of DME to a toluene solution of **5**, which results in the rapid precipitation of LiI. Filtration of these solutions, followed by recrystallization of **5** from Et_2O/hexanes, provides material free from salt.

The temperature dependent magnetization data for **5** was collected between 4−205 K. The effective magnetic moment of **5** varies with temperature, decreasing from 1.19 μ_B at 205 K to 0.96 μ_B at 4 K (Figure 5). This temperature response is consistent with that usually observed for U(V).[62,64,65,70,79] Curie−Weiss fitting ($\chi = C/(T - \theta)$) of the $1/\chi$ versus T data[51] between 120 and 205 K (see Supporting Information) provides an approximate room temperature μ_{eff} of 1.3 μ_B. This value is significantly lower than the free ion value of 2.54 μ_B,[70] and lower than the effective magnetic moments typically observed for U(V) (ca. 1.9−2.5) at room temperature.[51,62,64,65,70,79] The related hexa(amido) complex $[^nBu_4N][U(dbabh)_6]$ exhibits a rather large room temperature μ_{eff} of 3.7 μ_B, but its low temperature value (1.16 μ_B at 5 K) is comparable to that observed for **5**.[34] Reduced effective magnetic moments in U(V) have been ascribed to covalence,[62,64,65] and a similar effect may also account for the low μ_{eff} exhibited by **5**. We have also attempted to record the ESR spectrum for **5** in

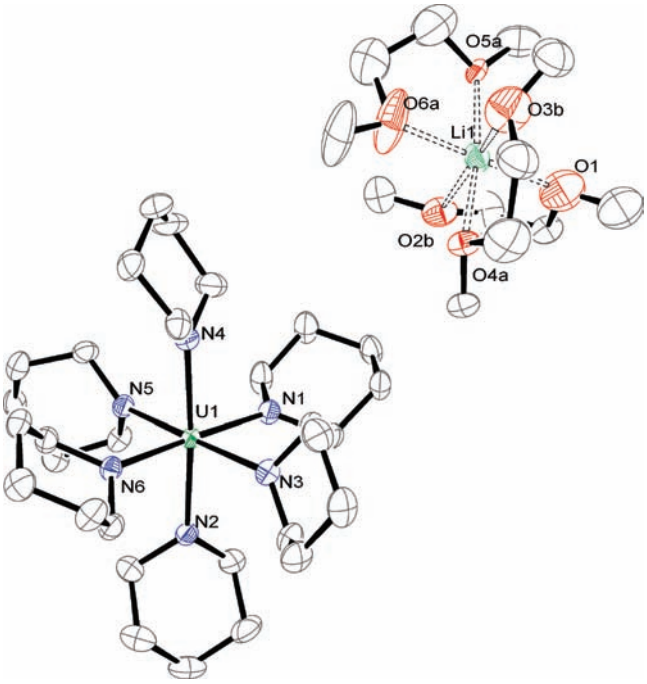

Figure 6. ORTEP diagram of $[Li(DME)_3][U(NC_5H_{10})_6]$ (**5**) with 50% probability ellipsoids. Selected bond lengths (Å) and angles (deg): U1−N1 = 2.292(6), U1−N2 = 2.266(6), U1−N3 = 2.250(6), U1−N4 = 2.280(6), U1−N5 = 2.283(6), U1−N6 = 2.270(5), N1−U1−N2 = 90.3(2), N1−U1−N3 = 86.3(2), N1−U1−N4 = 93.2(2), N1−U1−N5 = 88.9(2), N1−U1−N6 = 177.8(2). Sum of the angles around the nitrogen atoms: N1 = 359.5(8)°, N2 = 358.4(9)°, N3 = 359.5(9)°, N4 = 357.7(9)°, N5 = 359.7(9)°, N6 = 359.3(8)°.

2-methyltetrahydrofuran at 100 K; however, no signal was observed under these conditions.

The room temperature cyclic voltammogram of **5** in THF exhibits a reversible oxidation feature at −1.51 V (vs $[Cp_2Fe]^{0/+}$) (see the Supporting Information) which we have assigned to the U(VI/V) redox couple. Scanning to positive potentials produces two irreversible features that we attribute to ligand-based oxidation events. Additionally, reduction of **5** to U(IV) was not observed within the range of the solvent window. The U(VI/V) redox potential of **5** is lower than those recorded for related uranium alkoxide[27,80] and amide[34] complexes. For example, its reduction potential is 500 mV lower than that found for $[U(dbabh)_6]^{0/-}$ ($E_{1/2}$ = −1.01 V vs $[Cp_2Fe]^{0/+}$) and nearly 400 mV lower than that of $[U(O^tBu)_6]^{0/-}$ ($E_{1/2}$ = −1.12 V vs $[Cp_2Fe]^{0/+}$).[27,34] This data suggests that the piperidide ligand is a stronger donor than either $[dbabh]^-$ or $[O^tBu]^-$.

On the basis of our cyclic voltammetry results, we attempted the chemical oxidation of complex **5**. Addition of 0.5 equiv of I_2 to an Et_2O solution of **5** immediately generates a black solution from which the U(VI) piperidide complex $U(NC_5H_{10})_6$ (**6**) can be isolated in 51% yield by crystallization from hexane (Scheme 2). The LiI byproduct formed during the synthesis of **6** is also a challenge to completely remove, necessitating its precipitation with DME, as was done for complex **5**. The ^1H NMR spectrum of **6** in C_6D_6 consists of two resonances at 1.87 and 8.85 ppm, in a 3:2 ratio. The peak at 1.87 ppm is attributable to the β- and γ-proton resonances of the piperidide ligand, whereas the peak at

(78) Berthet, J. C.; Ephritikhine, M. *J. Chem. Soc., Chem. Commun.* **1993**, 1566–1567.
(79) Castro-Rodriguez, I.; Nakai, H.; Meyer, K. *Angew. Chem., Int. Ed.* **2006**, *45*, 2389–2392.
(80) Fortier, S.; Wu, G.; Hayton, T. W. *Inorg. Chem.* **2009**, *48*, 3000–3011.

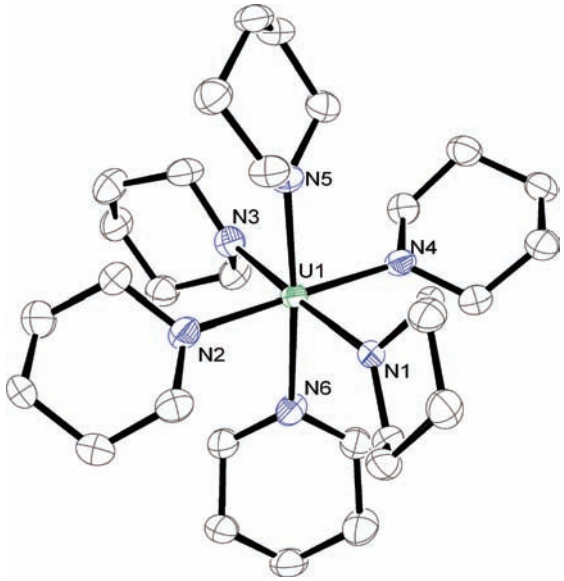

Figure 7. ORTEP diagram of $U(NC_5H_{10})_6$ (**6**) with 50% probability ellipsoids. Selected bond lengths (Å) and angles (deg): U1−N1 = 2.211(4), U1−N2 = 2.208(5), U1−N3 = 2.208(5), U1−N4 = 2.238(5), U1−N5 = 2.251(5), U1−N6 = 2.239(5), N1−U1−N2 = 91.5(2), N1−U1−N3 = 176.0(2), N1−U1−N4 = 87.6(2), N1−U1−N5 = 94.2(2), N1−U1−N6 = 86.6(2). Sum of the angles around the nitrogen atoms: N1 = 359.4(6)°, N2 = 358.2(8)°, N3 = 359.9(8)°, N4 = 359.4(7)°, N5 = 356.6(8)°, N6 = 357.4(7)°.

8.85 ppm is assignable to the α-protons. Solutions of **6** are stable for several hours at room temperature, differing from the reported instability of $U(NMe_2)_6$, which slowly decomposes to $U(NMe_2)_5$.[31]

Single crystals suitable for X-ray crystallographic analysis were grown from a dilute toluene solution stored at −25 °C. Complex **6** crystallizes in the monoclinic space group $P2_1/c$, and its solid-state molecular structure is shown in Figure 7. In the solid-state, complex **6** exhibits an octahedral geometry. Its U−N bond lengths (U1−N1 = 2.211(4) Å, U1−N2 = 2.208(5) Å, U1−N3 = 2.208(5) Å, U1−N4 = 2.238(5) Å, U1−N5 = 2.251(5) Å, U1−N6 = 2.239(5) Å) are nearly identical to those observed in **5**, decreasing by an average of only 0.05 Å, and similar to those of the U(VI) amide complex $U(dbabh)_6$ (U−N = 2.187(6) to 2.208(5) Å).[34] Its U−N bond distances are also comparable to the terminal $U-N_{amide}$ distances observed in the uranyl piperidide complex $[UO_2(NC_5H_{10})_3]_2^{2-}$ (av. terminal $U-N_{amide}$ = 2.25 Å).[26] Additionally, all six nitrogen atoms in **6** exhibit planar geometries, suggesting sp^2 hybridization.

Concluding Remarks

In this contribution we have demonstrated that homoleptic amide "-ate" complexes of U(IV) are accessible by reaction of UCl_4 with lithium amide salts. As with the homoleptic U(IV) alkyl complexes isolated previously by our group,[28] "-ate" complex formation is critical for imparting kinetic stability to the resulting uranium amido species: if only 4 equiv of the lithium amide are used during the synthesis, intractable mixtures are generated. Furthermore, both primary and secondary amide complexes are accessible by this route, as evidenced by the isolation of the *tert*-butylamide complex, $[Li(THF)_2Cl]_2$-$[Li]_2[U(NH^tBu)_6]$, and the piperidide complex, $[Li(DME)]$-$[U(NC_5H_{10})_5]$. However, the subsequent oxidation chemistry of these two materials differs significantly, revealing a difference between the reactivity of primary and secondary amides when ligated to a high-valent uranium center. In the case of $[U(NH^tBu)_6]^{2-}$, oxidation with either AgOTf or I_2 does not generate the intended U(VI) hexakis(amido) complex. Instead, a U(VI) bis(imido) complex is formed via deprotonation of two amido ligands. This process is no doubt driven by the formation of the strong U−N multiple bonds in the $[U(N^tBu)_2]^{2+}$ moiety. In contrast, oxidation of the secondary amide complex $[Li(DME)][U(NC_5H_{10})_5]$ by 0.5 equiv of I_2, followed by addition of 1 equiv of $LiNC_5H_{10}$, readily generates the target U(V) complex $[Li(DME)_3][U(NC_5H_{10})_6]$. The subsequent oxidation of this material yields the U(VI) derivative $U(NC_5H_{10})_6$. Complexes $[Li(DME)][U(NC_5H_{10})_5]$, $[Li(DME)_3][U(NC_5H_{10})_6]$, and $U(NC_5H_{10})_6$ offer an opportunity to examine the uranium−nitrogen bond in highly symmetric environment, in three oxidation states. Moreover, $U(NC_5H_{10})_6$ represents a relatively rare example of a U^{6+} complex with a non-uranyl ligand set. As such, $U(NC_5H_{10})_6$ may prove a valuable reagent for entry into further U^{6+} chemistry, and we are planning to explore the reactivity of this material with a variety of Al- and Zn-based alkyl transfer reagents. This would potentially provide access to U(VI) organometallic complexes, a class of materials which are essentially unknown.

Experimental Section

General Procedures. All reactions and subsequent manipulations were performed under anaerobic and anhydrous conditions either under a high vacuum or an atmosphere of argon or nitrogen. Diethyl ether, hexanes, toluene, and THF were dried using a Vacuum Atmospheres DRI-SOLV Solvent Purification system. DME was distilled from sodium benzophenone ketyl. All deuterated solvents were purchased from Cambridge Isotope Laboratories Inc. and were dried over activated 4 Å molecular sieves for 24 h prior to use. UCl_4 was synthesized according to the published procedures.[81] All other reagents were obtained from commercial sources and used as received.

NMR spectra were recorded on a Varian UNITY INOVA 500 spectrometer. ^1H and $^{13}C\{^1H\}$ NMR spectra are referenced to external $SiMe_4$ using the residual protio solvent peaks as internal standards (^1H NMR experiments) or the characteristic resonances of the solvent nuclei (^{13}C NMR experiments). $^7Li\{^1H\}$ NMR spectra are referenced to an external saturated solution of LiCl in deuterium oxide. Elemental analyses were performed by the Micro-Mass Facility at the University of California, Berkeley. IR spectra were recorded on a Mattson Genesis FTIR spectrometer. UV−vis/NIR spectra were recorded on a UV-3600 Shimadzu spectrophotometer.

Cyclic Voltammetry Measurements. CV experiments were performed using a CH Instruments 600c Potentiostat, and the data were processed using CHI software (version 6.29). All experiments were performed in a glovebox using a 20 mL glass vial as the cell. The working electrode consisted of a platinum disk embedded in glass (2 mm diameter), and both the working and reference electrodes consisted of platinum wire. Solutions employed during CV studies were typically 3 mM in the uranium complex and 0.1 M in $[Bu_4N][PF_6]$. All potentials are reported versus the $[Cp_2Fe]^{0/+}$ couple. For all trials, $i_{p,a}/i_{p,c} = 1$ for the $[Cp_2Fe]^{0/+}$ couple, while $i_{p,c}$ increased linearly with the square root of the scan rate (i.e., $\sqrt{v}$). Redox couples which exhibited behavior similar to the $[Cp_2Fe]^{0/+}$ couple were thus considered reversible.

(81) Kiplinger, J. L.; Morris, D. E.; Scott, B. L.; Burns, C. J. *Organometallics* **2002**, *21*, 5978–5982.

Magnetism Measurements. Magnetism data were recorded using a Quantum Design MPMS 5XL SQUID magnetometer. All experiments were performed between 4−300 K using 50−100 mg of powdered, crystalline solid. Complex **4** was loaded, under an inert atmosphere, into a Teflon-lined gelatin capsule and packed with approximately 20 mg of quartz wool. The sample was positioned within a plastic straw for analysis. The data were not corrected for the contribution of the gelatin capsule/straw sample holder. Complex **5** was loaded into an NMR tube, which was subsequently flame-sealed. The solid was kept in place with approximately 45 mg quartz wool packed on either side of the sample. The data were corrected for the contribution of the NMR tube holder and the quartz wool. The experiment for **4** was performed using a 1 T field, whereas the experiment for **5** was performed using a 5 T field. Diamagnetic corrections ($\chi_{dia} = -4.23 \times 10^{-4}$ cm^3·mol^{-1} for **4**, $\chi_{dia} = -5.98 \times 10^{-4}$ cm^3·mol^{-1} for **5**) were made using Pascal's constants.[82]

LiNH^{t}Bu. To a solution of *tert*-butylamine (3.0 mL, 28.4 mmol) in hexanes (30 mL) was added *n*-BuLi (1.6 M in hexanes, 17.0 mL, 27.2 mmol) dropwise via syringe. The reaction mixture was stirred for 24 h whereupon the solvent was removed in vacuo to yield a white powder. 2.084 g, 93% yield. ^{1}H NMR (500 MHz, 25 °C, C_6D_6): δ 11.03 (s, 1H, NH), 1.36 (s, 9H, CH_3). ^{7}Li{^{1}H} NMR (194 MHz, 25 °C, C_6D_6): δ 0.03 (s).

LiNC$_5$H$_{10}$. To a solution of piperidine (3.0 mL, 30.4 mmol) in hexanes (20 mL) at 0 °C was added *n*-BuLi (1.6 M in hexanes, 19.0 mL, 30.4 mmol) dropwise via syringe. This resulted in the immediate precipitation of an off-white solid. After stirring for 24 h, the solution was allowed to settle, and the supernatant was decanted off. The solid was dried in vacuo to give a white powder. 2.482 g, 90% yield. ^{1}H NMR (500 MHz, 25 °C, C_6D_6): δ 3.33 (m, 4H, CH_2), 1.96 (m, 2H, CH_2), 1.68 (m, 4H, CH_2). ^{7}Li{^{1}H} NMR (194 MHz, 25 °C, C_6D_6): δ −1.52 (s).

[Li(THF)$_2$Cl]$_2$[Li]$_2$[U(NH^{t}Bu)$_6$] (1·THF). To a cold (−25 °C), stirring solution of UCl_4 (0.098 g, 0.26 mmol) in THF (3 mL) was added a solution of LiNH^{t}Bu (0.125 g, 1.58 mmol) in THF (3 mL) dropwise. The reaction mixture immediately turned orange-brown concomitant with the precipitation of a white solid. After stirring for 10 min, the solution was filtered through a Celite column (2 cm × 0.5 cm) supported on glass wool. To the filtrate was added DME (2 mL), and the solution was layered with hexanes (6 mL) and stored at −25 °C for 24 h, resulting in the deposition of orange crystals. The crystals were washed with hexanes (2 × 2 mL) and dried under vacuum. 0.157 g, 57% yield. ^{1}H NMR (500 MHz, 25 °C, C_6D_6): δ −20.42 (s, 6H, NH), 1.37 (s, 16H, β-THF), 2.10 (s, 54H, CCH_3), 3.54 (s, 16H, α-THF protons). ^{1}H NMR (500 MHz, 25 °C, THF-d_8): δ −21.03 (s, 6H, NH), 1.77 (s, 54H, CCH_3). ^{7}Li{^{1}H} NMR (194 MHz, 25 °C, C_6D_6): δ 0.93 (s). Anal. Calcd for $C_{40}H_{92}Cl_2Li_4N_6O_4U$: C, 45.41; H, 8.77; N, 7.94. Found: C, 45.03; H, 8.79; N, 7.73. Complex **1**·DME was synthesized similarly, but the crystals were grown by vapor diffusion of hexanes into a solution of **1**·THF dissolved in DME.

[Li(THF)]$_2$[U(N^{t}Bu)$_2$(NH^{t}Bu)$_4$] (2). To a suspension of **1**·THF (0.077 g, 0.073 mmol) in Et_2O (3 mL) was added AgOTf (0.019 g, 0.074 mmol) with stirring. Upon addition, the reaction mixture immediately turned dark brown concomitant with the deposition of a fine black precipitate. After 5 min, the solution was filtered through a Celite column (2 cm × 0.5 cm) supported on glass wool. The volume of the filtrate was reduced to 2 mL in vacuo, and the solution was subsequently layered with hexanes (3 mL). Storage of the solution at −25 °C for 24 h resulted in the deposition of red crystals. 0.020 g, 33% yield. ^{1}H NMR (500 MHz, 25 °C, C_6D_6): δ 1.08 (s, 18H, imido CH_3), 1.34 (s, 8H, β-THF protons), 2.06 (s, 36H, amide CH_3), 3.66 (s, 8H, α-THF protons), 4.82 (s, 4H, NH). ^{7}Li{^{1}H} NMR (194 MHz, 25 °C, C_6D_6): δ 1.52 (s). ^{13}C{^{1}H} NMR (125 MHz, 25 °C, C_6D_6): δ 25.28 (THF), 38.22 (s, CCH_3), 39.19 (s, CCH_3), 56.37 (THF), 58.66 (s, CCH_3). One CCH_3 resonance was not be observed. Anal. Calcd. $C_{32}H_{74}Li_2N_6O_2U$: C, 46.47, H, 9.04, N, 10.16. Found: C, 38.18, H, 7.22, N 7.27. The low carbon content is attributed to the presence of LiOTf in the sample, which we were unable to completely remove by recrystallization. IR (KBr pellet, cm^{-1}): 1457(s), 1409(w), 1376(m), 1351(s), 1313(w), 1296(w), 1207(s), 1186(s), 1113(w), 1039(s), 993(w), 982(w), 945(s), 891(s), 843(w), 789(m), 756(m), 719(m), 569(s), 542(s), 523(s), 474(s), 447(s), 411(w).

U(N^{t}Bu)$_2$(NH^{t}Bu)$_2$(NH$_2^t$Bu)$_2$ (3). To a stirring suspension of **1**·THF (0.352 g, 0.332 mmol) in Et_2O (8 mL) and ^{t}BuNH$_2$ (0.5 mL) was added a solution of I_2 (0.085 g, 0.334 mmol) in Et_2O (1 mL) dropwise. The reaction mixture immediately turned red concomitant with precipitation of a white powder. The solution was stirred for 5 min, whereupon the solvent was removed in vacuo, affording a red solid. The solid was dissolved in hexanes (3 mL), and the solution was filtered through a Celite column (2 cm × 0.5 cm) supported on glass wool. The solvent was then removed in vacuo to give a red microcrystalline powder. 0.175 g, 78% yield. ^{1}H NMR (500 MHz, 25 °C, C_6D_6): δ 0.90 (s, 18H, imido CH_3), 1.50 (s, 18H, amine CH_3), 1.97 (s, 18H, amide CH_3), 3.24 (s, 4H, amine NH), 10.16 (s, 2H, amide NH). ^{13}C{^{1}H} NMR (125 MHz, 25 °C, C_6D_6): δ 33.44 (s, CCH_3), 38.07 (s, CCH_3), 39.61 (s, CCH_3), 50.52 (s, CCH_3), 62.29 (s, CCH_3), 73.4(s, CCH_3). Anal. Calcd for $C_{24}H_{60}N_6U$: C, 42.96; H, 9.03; N, 12.52. Found: C, 42.72; H, 9.18; N 12.23. IR (KBr pellet, cm^{-1}): 1579(s), 1541(w), 1504(w), 1473(s), 1458(sh), 1420(w), 1395(m), 1370(s), 1351(s), 1324(w), 1298(w), 1256(m), 1220(s), 1212(s), 1187(s), 1124(w), 1118(sh), 1053(s), 984(s), 959(s), 926(m), 912(s), 893(sh), 818(w), 792(m), 779(w), 765(m), 749(w), 670(m), 560(s), 520(s), 477(s), 406(w).

[Li(DME)][U(NC$_5$H$_{10}$)$_5$] (4). To a cold (−25 °C), stirring solution of LiNC$_5$H$_{10}$ (0.589 g, 6.47 mmol) in Et_2O (8 mL) was added a suspension of UCl_4 (0.410 g, 1.08 mmol) in DME (5 mL) dropwise. The reaction mixture immediately turned blue-green concomitant with the precipitation of a white powder. The mixture was allowed to stir at room temperature for 30 min, whereupon the solvent was removed in vacuo affording a blue-green powder. The solid was dissolved in Et_2O (12 mL), and the solution was filtered through a Celite column (2 cm × 0.5 cm) supported on glass wool. The volume of the filtrate was reduced in vacuo, and the solution cooled to −25 °C for 24 h, resulting in the deposition of blue-green crystals. The crystals were washed with hexanes (2 × 2 mL) and dried under vacuum. 0.508 g, 62% yield. ^{1}H NMR (500 MHz, 25 °C, C_6D_6): δ 0.51 (s, 6H, DME), 6.24 (br s, 50H, fwhm = 1600 Hz, piperidide protons), 11.25 (s, 4H, DME). ^{7}Li{^{1}H} NMR (194 MHz, 25 °C, C_6D_6): δ 81.2 (s). Anal. Calcd for $C_{29}H_{60}LiN_5O_2U$: C, 46.08; H, 8.02; N, 9.27. Found: C, 45.94; H, 9.00; N, 8.21. UV−vis/NIR (THF, 7.38 mM, 25 °C, L·mol^{-1}·cm^{-1}): 456 (ε = 52.1), 462 (ε = 48.1), 528 (ε = 18.5), 534 (ε = 19.4), 580 (ε = 32.8), 608 (sh, ε = 22.5), 626 (ε = 36.3), 690 (ε = 16.0), 724 (ε = 10.1), 794 (ε = 18.7), 852 (ε = 44.1), 918 (ε = 54.7), 1038 (ε = 19.4), 1100 (ε = 11.8), 1204 (ε = 51.2), 1326 (ε = 13.1), 1452 (ε = 18.5), 1662 (ε = 38.7), 1778 (ε = 54.2), 1796 (ε = 68.9), 1814 (ε = 69.1), 1890 (ε = 33.4).

[Li(DME)$_3$][U(NC$_5$H$_{10}$)$_6$] (5). To a cold (−25 °C), stirring solution of **4** (0.325 g, 0.430 mmol) in Et_2O (8 mL) was added a solution of I_2 (0.057 g, 0.22 mmol) in Et_2O (2 mL) dropwise. This resulted in the immediate color change from blue-green to black. The reaction mixture was stirred for 5 min, whereupon a solution of LiNC$_5$H$_{10}$ (0.040 mg, 0.44 mmol) in Et_2O (8 mL) was added dropwise, causing the solution to turn deep red. The reaction mixture was then stirred for an additional 5 min, after which the solvent was removed in vacuo, affording a dark red solid. Dissolution of the solid in toluene (5 mL) followed by addition of DME (0.25 mL) resulted in the immediate precipitation of LiI(DME)$_2$ as a colorless solid. The solution was then filtered through a Celite column (2 cm × 0.5 cm) supported on

(82) Bain, G. A.; Berry, J. F. *J. Chem. Educ.* **2008**, *85*, 532.

Table 1. X-ray Crystallographic Data for Complexes **1**·THF, **1**·DME·C_6H_{14}, **2**, **4**–**6**

	1·THF	**1**·DME·C_6H_{14}	**2**
empirical formula	$C_{40}H_{92}Cl_2Li_4N_6O_4U$	$C_{46}H_{108}Cl_2Li_4N_6O_8U$	$C_{32}H_{74}Li_2N_6O_2U$
crystal habit, color	rod, orange	plate, brown	block, red
crystal size (mm)	0.50 × 0.20 × 0.15	0.60 × 0.50 × 0.20	0.14 × 0.12 × 0.10
crystal system	monoclinic	triclinic	monoclinic
space group	$P2_1/n$	$P\bar{1}$	$C2/m$
volume (Å^3)	2745.8(3)	1619(1)	2034.3(7)
a (Å)	10.6583(6)	10.866(5)	16.380(3)
b (Å)	19.162(1)	11.072(5)	14.155(3)
c (Å)	13.8312(8)	14.719(7)	11.978(3)
α (deg)	90	78.666(7)	90
β (deg)	103.576(2)	77.331(7)	132.903(4)
γ (deg)	90	71.050(7)	90
Z	2	1	2
formula weight (g/mol)	1057.89	1210.07	826.88
density (calculated) (Mg/m^3)	1.280	1.241	1.350
absorption coefficient (mm^{-1})	3.091	2.634	4.021
F_{000}	1088	628	844
total no. reflections	6891	12280	7929
unique reflections	4414	5847	2106
final R indices [$I > 2\sigma(I)$]	R_1 = 0.0447, wR_2 = 0.1099	R_1 = 0.0408, wR_2 = 0.1081	R_1 = 0.0355, wR_2 = 0.0769
largest diff. peak and hole (e$^-$ Å^{-3})	3.104 and −1.656	2.081 and −2.610	1.444 and −0.555
GOF	0.938	1.025	0.965

	4	**5**	**6**
empirical formula	$C_{29}H_{60}LiN_5O_2U$	$C_{42}H_{90}LiN_6O_6U$	$C_{30}H_{60}N_6U$
crystal habit, color	rhombus, blue-green	block, dark red	block, black
crystal size (mm)	0.70 × 0.60 × 0.50	0.70 × 0.70 × 0.30	0.30 × 0.30 × 0.20
crystal system	hexagonal	monoclinic	monoclinic
space group	$P3_2$	$P2_1/n$	$P2_1/c$
volume (Å^3)	2498(4)	4873.1(8)	3124.4(7)
a (Å)	11.261(9)	15.173(1)	10.386(1)
b (Å)	11.261(9)	18.775(2)	17.154(2)
c (Å)	22.75(2)	17.123(2)	17.858(2)
α (deg)	90	90	90
β (deg)	90	92.492(1)	100.896(2)
γ (deg)	120	90	90
Z	3	4	4
formula weight (g/mol)	755.79	1020.17	742.87
density (calculated) (Mg/m^3)	1.507	1.391	1.579
absorption coefficient (mm^{-1})	4.905	3.378	5.223
F_{000}	1140	2108	1496
total no. reflections	19951	40711	25724
unique reflections	6732	10142	6295
final R indices [$I > 2\sigma(I)$]	R_1 = 0.0611, wR_2 = 0.1530	R_1 = 0.0444, wR_2 = 0.1254	R_1 = 0.0364, wR_2 = 0.0778
largest diff. peak and hole (e$^-$ Å^{-3})	5.723 and −1.616	3.407 and −1.776	3.235 and −1.371
GOF	1.050	1.055	1.020

glass wool. The solvent was removed in vacuo, and the resulting red solid was subsequently dissolved in Et_2O (4 mL). The solution was layered with hexanes (4 mL) and stored at −25 °C for 24 h, resulting in the formation of dark red blocks. The crystals were washed with hexanes (2 × 2 mL) and dried under vacuum. 0.231 g, 53% yield. ^{1}H NMR (500 MHz, 25 °C, C_6D_6): δ 2.48 (s, 24 H, piperidide β-protons), 2.56 (s, 12H, piperidide γ-protons), 3.30 (s, 18H, DME), 3.48 (s, 12H, DME), 11.59 (br s, 24 H, piperidide α-protons). ^{7}Li{^{1}H} NMR (194 MHz, 25 °C, C_6D_6): δ 13.5 ppm. Anal. Cald for $C_{42}H_{90}LiN_6O_6U$: C, 49.40; H, 8.91; N, 8.24. Found: C, 49.68; H, 8.67; N, 8.40. UV−vis/NIR (THF, 6.36 mM, 25 °C, L·mol^{-1}·cm^{-1}): 746 (sh, ε = 43.7), 848 (ε = 38.6), 932 (ε = 43.1), 1458 (ε = 16.3).

[U(NC$_5$H$_{10}$)$_6$] (6). To a cold (−25 °C), stirring solution of **5** (0.147 g, 0.144 mmol) in Et_2O (8 mL) was added a solution of I_2 (0.019 g, 0.075 mmol) in Et_2O (2 mL) dropwise. The reaction mixture immediately turned black. After stirring for 5 min, the solvent was removed in vacuo affording a black solid. Dissolution of the solid in toluene (5 mL) followed by addition of DME (0.25 mL) resulted in the immediate precipitation of $LiI(DME)_2$ as a colorless solid. The solution was then filtered through a Celite column (2 cm × 0.5 cm) supported on glass wool. The solvent was removed in vacuo, and the resulting black solid was subsequently dissolved in hexanes (4 mL). Storage of the hexanes solution at −25 °C for 24 h resulted in the deposition of black microcrystalline powder. X-ray quality crystals of **7** were grown from a dilute toluene solution stored at −25 °C for 24 h. 0.054 g, 51% yield. ^{1}H NMR (500 MHz, 25 °C, C_6D_6): δ 1.87 (s, 36H, piperidide β- and γ-protons), 8.85 (s, 24H, piperidide α-protons). ^{13}C{^{1}H} NMR (125 MHz, 25 °C, C_6D_6): δ 23.88 (s, γ-CH_2), 39.57 (s, β-CH_2), 50.18 (s, α-CH_2). Anal. Calcd for $C_{30}H_{60}N_6U$: C, 48.49; H, 8.16; N, 11.30. Found: C, 48.29; H, 7.93; N, 10.96.

X-ray Crystallography. Data for **1**·THF, **1**·DME·C_6H_{14}, **2**, **4**–**6** were collected on a Bruker 3-axis platform diffractometer equipped with a SMART-1000 CCD detector using a graphite monochromator with a Mo Kα X-ray source (α = 0.71073 Å). The crystals were mounted on a glass fiber under Paratone-N oil and all data was collected at 150(2) K using an Oxford nitrogen gas cryostream system. A hemisphere of data was collected using ω scans with 0.3° frame widths. Frame exposures of 10 s were used for **1**·THF, **1**·DME·C_6H_{14}, **4**–**6**, while frames exposures of 20 s were used for **2**. Data collection and cell parameter determination were conducted using the SMART program.[83]

(83) *SMART Software Users Guide*, Version 5.1; Bruker Analytical X-Ray Systems, Inc.: Madison, WI, 1999.

Integration of the data frames and final cell parameter refinement were performed using SAINT software.[84] Absorption correction of the data was carried out empirically based on reflection ψ-scans. Subsequent calculations were carried out using SHELXTL.[85] Structure determination was done using direct or Patterson methods and difference Fourier techniques. All hydrogen atom positions were idealized, and rode on the atom of attachment with exceptions noted in the subsequent paragraph. Structure solution, refinement, graphics, and creation of publication materials were performed using SHELXTL.[85] Additionally, structure **2** possessed a disordered THF molecule which was modeled in two positions with occupancies of 0.5 each. Atoms of the DME molecules in **5** also exhibited positional disorder. This was addressed by modeling these atoms in two positions with occupancies of 0.5 each. Idealized hydrogens were not assigned to the disordered carbon atoms of **2** or **5**. A summary of relevant crystallographic data for **1**·THF, **1**·DME·C_6H_{14}, **2**, **4**−**6** is presented in Table 1.

(84) *SAINT Software User's Guide*, Version 5.1; Bruker Analytical X-Ray Systems, Inc.: Madison, WI, 1999.

(85) Sheldrick, G. M. *SHELXTL*, 6.12; Bruker Analytical X-Ray Systems, Inc.: Madison, WI, 2001.

Acknowledgment. We thank the University of California, Santa Barbara and the Department of Energy (BES Heavy Element Program) for financial support of this work. S.F. was supported in part by a Graduate Opportunity Fellowship from UCSB.

Supporting Information Available: Experimental procedures, crystallographic details (as CIF files), magnetic susceptibility plots, tabulated cyclic voltammetry data and spectral data for **1**−**6**. This material is available free of charge via the Internet at http://pubs.acs.org.